Chemical Characteristics and Brown Carbon Chromophores of Atmospheric Organic Aerosols Over the Yangtze River Channel: A Cruise Campaign

X. Wang, N. Hayeck, M. Bruggemann, L. Abis, M. Riva, Y. Lu, Biao Wang, J. Chen, C. George, L. Wang

Chemical characteristics and brown carbon chromophores of atmospheric organic aerosols over the Yangtze River channel: a cruise campaign

Xinke Wang[1,2], Nathalie Hayeck[2$], Martin Brüggemann[3], Letizia Abis[2], Matthieu Riva[2], Yiqun Lu[1], Buwei Wang[4], Jianmin Chen[1], Christian George[2 *], Lin Wang[1,5,6 *]

[1] *Shanghai Key Laboratory of Atmospheric Particle Pollution and Prevention (LAP[3]), Department of Environmental Science & Engineering, Jiangwan Campus, Fudan University, Shanghai 200438, China*

[2] *Univ Lyon, Université Claude Bernard Lyon 1, CNRS, IRCELYON, F-69626, Villeurbanne, France*

[3] *Leibniz Institute for Tropospheric Research (TROPOS), Atmospheric Chemistry Department (ACD), Permoserstr. 15, 04318 Leipzig, Germany*

[4] *State Key Laboratory of Operation and Control of Renewable Energy & Storage Systems, China Electric Power Research Institute. Beijing 100192, China*

[5] *Collaborative Innovation Center of Climate Change, Nanjing 210023, China*

[6] *Shanghai Institute of Pollution Control and Ecological Security, Shanghai 200092, China*

[$] *Now at the Chemistry Department, Faculty of Arts and Sciences, American University of Beirut, Beirut, Lebanon*

* *Corresponding Authors: C.G., email, Christian.George@ircelyon.univ-lyon1.fr; phone, (33)(0)437423681; fax, (33)(0)472448438. L.W., email, lin_wang@fudan.edu.cn; phone, +86-21-31243568.*

Key Points:

(1) More than one thousand atmospheric particulate organics including seventy-six BrC chromophores were determined over the Yangtze River channel.

(2) Brown carbon chromophores exhibit high degrees of unsaturation, suggesting being aromatics, nitro-aromatics, or polycyclic aromatics.

(3) Biomass burning tracers contribute significantly to the total light absorption of organic aerosols.

Abstract.

Organic aerosols (OAs) have important influences on the climatic implications and health effects of atmospheric aerosols. Among the complex OA constituents, brown carbon (BrC) accounts for a substantial mass fraction and is of special interest because of its light-absorbing properties. In this study, the chemical composition of atmospheric OAs over the middle-lower Yangtze River (MLYR) channel, as well as the BrC, was investigated during a ship cruise campaign in winter 2015. In total, more than one thousand molecular formulas were determined using a combination of ultra-high performance liquid chromatography (UHPLC), a diode array detector (DAD), and Orbitrap high-resolution mass spectrometry (HRMS). Large numbers and enhanced signal abundances for known tracers as well as monocyclic and polycyclic aromatics indicate that biomass burning and fossil combustion are important sources of OAs over the MLYR channel. In addition, thirteen chromophores with strong light absorption, mostly representing established biomass burning tracers, were unambiguously determined by UHPLC/DAD/HRMS and contributed to 35-37% of the total light absorption of OAs at 290 nm and 58-70% at 350 nm. Sixty-three previously identified biomass burning chromophores were also positively identified in the mass spectrometric analysis here but embedded in the humped signal during the spectroscopic analysis. These BrC chromophores exhibit high degrees of unsaturation, suggesting these compounds to be aromatic, nitro-aromatic, and polycyclic aromatic type of species. Our results highlight the significant influence of biomass burning and fossil combustion on atmospheric OAs over the MLYR channel in the winter, strongly

enhancing light-absorbing properties and decreasing air quality.

1. Introduction

Organic aerosols (OAs) contribute to around 20-50% of the submicron particulate mass in continental mid-latitudes and can account for as much as 90% of the particulate mass in tropical forested areas, exerting important influences on climatic processes and human health (Andreae & Crutzen, 1997; Kanakidou et al., 2005). OAs can be released through direct emissions from natural or anthropogenic sources and/or formed in the atmosphere through chemical reactions of volatile organic compounds (VOCs) and the subsequent gas-to-particle conversion of less volatile reaction products (Pöschl, 2005). In addition to their diverse sources, the multiple chemical reactions of OA components can significantly increase their complexity (Goldstein & Galbally, 2007). Eventually, these OA components impact the physicochemical properties and the potential toxicity of OAs (Ito et al., 2019; Lei et al., 2014; Tang et al., 2016).

Light-absorbing OA components, typically referred to as brown carbon (BrC), exhibiting strong light absorption in the near-ultraviolet (UV) and visible wavelength regions, thus, affecting climate forcing properties of aerosol particles (Bahadur et al., 2012; Chung et al., 2012). The study of Feng et al. (2013) concluded that the radiative forcing of climate by BrC can contribute up to +0.25 W m^{-2}, higher than 25% of that by black carbon (BC). Released from both fossil fuel and biomass burning, BC represents soot-like particles with a broad light absorption from the UV up to the infrared wavelength range and may be the second most important atmospheric

component for global warming in terms of direct forcing (Jacobson, 2001). It also showed that BrC may be the dominant atmospheric light-absorbing material over the regions of biomass burning and biofuel combustion such as South and East Asia, South America, and subtropical Africa (Feng et al., 2013). In addition, global models concluded that the absorption of solar radiation by BrC was 27%-70% of that by BC (Lin et al., 2018). Moreover, the BrC absorption was shown to explain almost 30% of the total aerosol absorption at 370 nm (Yang et al., 2009), and even at 550 nm to be as high as 20% (Chung et al., 2012).

BrC constituents, compared to BC, are less characterized due to their complex composition and properties (Andreae & Gelencsér, 2006). BrC is present in both primary aerosols, emitted from combustion processes, and secondary organic aerosols (SOAs). Several studies have idenfied a wide variety of light-absorbing chromophores, including nitro-aromatics, polycyclic aromatic hydrocarbon derivatives, polyphenols, and sulfur-containing compounds, by investigating the molecular composition of freshly emitted biomass burning OAs (Budisulistiorini et al., 2017; Lin et al., 2016; Fleming et al., 2018). The exact chemical composition and physicochemical properties of light-absorption BrC chromophores are related to the fuel type that is burned (Chakrabarty et al., 2010; Iinuma et al., 2007; Lin et al., 2016). Secondary BrC were shown to be generated from multiphase chemistry, such as acid-catalyzed aldol condensation, nitration of aromatic compounds, and the reactions of ammonium ions and amino acids with carbonyls and dicarbonyls (Bones et al., 2010; De Haan et al., 2009; Kampf et al., 2016; Kwamena & Abbatt, 2008; Shapiro et al., 2009). Furthermore,

numerous lab studies have shown that atmospheric processing such as solar irradiation, oxidation, and changes in temperature and relative humidity can alter the composition of BrC and significantly change their optical properties (Lambe et al., 2012; Lee et al., 2013; Lee et al., 2014; Nguyen et al., 2012; Rincón et al., 2010; Zhao et al., 2015). For example, Lee et al. (2014) show that SOAs formed from the photo-oxidation of naphthalene under high NOx and from the reaction of limonene with ozone (O_3) could be potential sources of secondary BrC, but would "photobleach" meaning lose their near-UV absorbance after solar radiation with effective half-lives of ~14 h and <0.5 h, respectively. Therefore, based on the local emissions and atmospheric conditions at a specific geographic location, the chemical composition and physicochemical properties of atmospheric BrC components can be very different.

The Yangtze River is the longest river in China and passes by several highly developed economic megacities with major petrochemical complexes and/or steel industries (Li et al., 2018), leading to high emissions of anthropogenic pollutants including particulate matters, VOCs, sulfur dioxide, and nitrogen oxides (Huang et al., 2011). Meanwhile, the Yangtze River also plays an important role in shipping of goods and leisure cruising. Therefore, atmospheric OAs produced/formed over the Yangtze River channel are expected to be complex including abundant BrC components.

Here, we collected filter samples of atmospheric particles during a cruise campaign carried out along the MLYR channel from November to December 2015 (i.e., Yangtze River Campaign, YRC), and analyzed the samples to characterize their organic fraction.

In addition, light-absorbing BrC chromophores in the complex OAs were identified via connection of mass spectrometric analysis and spectroscopic analysis. The relative contribution of the strongest BrC chromophores to the total light absorption of OAs was also evaluated. The results obtained help not only to better understand the sources and physicochemical properties of atmospheric aerosols, but also to further characterize the constituents of air pollution at a molecular level over the MLYR channel region.

2. Material and methods

2.1 Collection of $PM_{2.5}$ samples

Atmospheric aerosol samples were collected onto 90 mm prebaked quartz-fiber filters (Whatman Company, UK) using a middle-flow aerosol sampler (Qingdao Hengyuan Tech Co., Ltd., HY-100) for six hours at a flow rate of 100 L min^{-1}, from November 22nd to December 5th, 2015 along the Yangtze River channel between Shanghai and Wuhan (Figure 1). Details about the YRC can be found in a previous study (Li et al., 2018). In order to avoid the possible contaminations from self-emission of the ship, the sampler was placed on the bow of the research vessel. In addition, only filter samples during the time period with relative wind directions between -100° and 100° of the moving direction of the ship and with a relative wind speed of >1.0 m s^{-1} were selected for further analysis. As a result, six samples with sample IDs of 1201M, 1201A, 1201N, 1202M, 1202N, and 1203A, respectively, were selected, where the numbers represent the sampling date, M denotes “morning”, A denotes “afternoon”, and N denotes “night”. Figure 1 and Table 1 show the route of the vessel during the

campaign and the start and end locations of these six samples. Field blank filters were collected by placing prebaked quartz-fiber filters into a parallel sampler for one hour without any air flow through the filter substrate. After collection, all filters were stored at -20°C in a freezer until further analysis to avoid changes in aerosol composition.

2.2 Aerosol sample analysis

Detailed procedures for sample filter extraction can be found in previous studies (Wang et al., 2017; Wang et al., 2016). Briefly, a quarter of each quartz filter was extracted twice with 6 mL of acetonitrile (Optima® LC/MS, Fischer Scientific, USA) and agitated for 20 min. Then the combined extracts were filtered through a 0.2 μm polytetrafluoroethylene membrane (13 mm, Pall Corporation, USA), and concentrated under a gentle stream of N_2. The extracts were then reconstituted in 1 mL of a 1:1 vol/vol mixture of water (Optima® LC/MS, Fischer Scientific, USA) and acetonitrile. Lastly, 200 μL of the reconstituted extract was diluted by adding 100 μL of water before further analysis due to the high concentrations of organics.

Then the diluted extracts were analyzed by an UHPLC/DAD/HRMS platform, which is the combination of ultra-high performance liquid chromatography (UHPLC, Dionex 3000, Thermo Scientific, USA), a diode array detector (DAD, Dionex UltiMate3000, Thermo Scientific, USA), and Orbitrap high resolution mass spectrometry (HRMS, Q Exactive, Thermo Scientific, Bremen, Germany) using heated electrospray ionization (HESI). Three replicate analyses were performed for each sample extract. The separation was performed using a Waters Acquity HSS T3 column (1.8 μm, 100 × 2.1

mm), and the procedures of gradient elution were described in earlier studies (Wang et al., 2017; Wang et al., 2016). In this study, the UV-Vis absorption was measured using a DAD over the wavelength range of 280-480 nm with low baseline noise (< ±10 μAU at 254 nm) and high linearity up to 2.0 AU. For the HRMS analysis, HESI voltages of -2.6 and 3.2 kV were applied in negative and positive ionization mode (ESI- and ESI+) measurements, respectively. The sheath gas flow rate was 42 arbitrary units (a.u.) and the auxiliary gas flow rate was 25 a.u. The temperature of the Orbitrap capillary temperature was set at 350 °C and the temperature of the HESI source at 250 °C. The mass resolving power of the Q-Exactive mass spectrometer was 140 000 at *m/z* 200, and a 2 mM sodium acetate solution was used to provide a series of negative and positive adduct ions in the scanning range of *m/z* 50–750 Th to perform the daily external mass calibration.

Pentafluorobenzylhydroxylamine (PFBHA) derivatization was used to identify organic compounds with carbonyl functional group(s) (Borrás & Tortajada-Genaro, 2012). 200 μL of the reconstituted extract were mixed with 800 μL of o-(2, 3, 4, 5, 6-pentafluorobenzyl) hydroxylamine hydrochloride (Sigma Aldrich, ≥ 99.0%) solutions (1 mg/mL). The mixtures were then left in darkness at room temperature for 24 h, and analyzed following the same procedure as earlier described in this session.

2.3 Data processing

Data were acquired using Xcalibur 2.2 (Thermo, USA). The subsequent non-target screening approach was conducted using an MZmine 2.33 software package. Molecular

formulas were assigned to detected signals satisfying the following constraints: $C_{1-50}H_{0-100}O_{0-40}N_{0-5}S_{0-3}$ ($C_{1-50}H_{0-100}O_{0-40}N_{0-5}S_{0-3}F_{0-20}$ for PFBHA derivatives analysis) with a mass tolerance of 2 ppm in ESI- and 3 ppm in ESI+; element count heuristics (i.e., H/C ratio ($0.3 \leq H/C \leq 3$); NOPS/C ratios ($N/C \leq 4$, $O/C \leq 3$, $P/C \leq 2$, $S/C \leq 3$); multiple element counts (if each of N, O, P, and S > 1 then N< 10, O < 20, P < 4, S < 3; if each of N, O, and P > 3 then N < 11, O < 22, P < 6; if each of O, P, and S > 1 then O < 14, P < 3, S < 3; if each of P, S, and N > 1 then P < 3, S < 3, N < 4; if each of N, O, and S > 6 then N < 19, O < 14, S < 8), ring and double bond equivalence (RDBE) restrictions (in the range of 0-25), and isotope pattern matching. It should be noted that the CAMERA algorithm was applied in order to avoid false detection from interferences of multiply charged ions and adducts (Kuhl et al., 2012). Further details on the LC-MS data processing are listed in Tables S1-S2.

In addition to RDBE, aromaticity equivalents (Xc) and Kendrick mass defect (KMD) values were calculated, and more details about the calculation can be found in the supplemental Text S1 and from our previous study (Wang et al., 2017). Xc has been suggested to help identification and characterization of monocyclic and polycyclic aromatic compounds, with $Xc \geq 2.50$ and $Xc \geq 2.71$ as unambiguous minimum criteria for the presence of mono- and polycyclic aromatic compounds, respectively (Yassine et al., 2014). KMD is useful to differentiate groups of similar compounds among a large set of molecular formulas. In this study, CH_2 was chosen as a base unit, and thus, molecules with identical KMDs differ only in the number of $–CH_2$ groups (Hughey et al., 2001).

The assigned formulas were subdivided into seven groups: compounds containing only carbon, hydrogen, and oxygen atoms in the ESI- and ESI+ (hereafter referred to as CHO- and CHO+, respectively); nitrogen-containing organics (hereafter referred to as CHON- and CHON+, respectively); sulfur-containing organics and compounds containing both nitrogen and sulfur in ESI- (hereafter referred to as CHOS- and CHONS-, respectively); and finally, organics without oxygen in ESI+ (hereafter referred to as CHN+). Similarly to our previous study (Wang et al., 2017), CHOS+ and CHONS+ compounds were also observed but accounted merely for a few percentages, so they were not further considered here.

It should also be noted that although LC separation might help reducing ion suppression effects, only a semi-quantification of organic compounds can be proposed. Using ESI, significant uncertainties originate also from different ionization efficiencies of particulate organic components which typically exhibit a wide range of different structures and functional groups (Lin et al., 2012). Due to the large variety of compounds and the technical impossibility of providing calibration factors for individual species, we assumed that the determined compounds have a similar signal response and the total peak areas of organics can be compared among different samples.

3. Results and discussion

3.1 Organic aerosols over the MLYR channel

In this study, 695-1187 and 450-695 molecular formulas were determined in ESI- and ESI+, respectively (Table 1). Due to the inherent differences in the ionization

mechanisms between ESI- and ESI+, a minor fraction of the detected compounds appears in both modes as shown by the formula lists (see Dataset 1). Data from ESI- and ESI+ can provide complementary information to characterize the molecular composition of complex OAs (Lin et al., 2018). However, non-polar compounds, which may be part of BrC, are difficult to be ionized by ESI (Kuang et al., 2018). Therefore, contributions from non-polar compounds might be underestimated in this study. The number and percentage of molecular formulas for each subgroup tentatively identified in each sample were listed in Table 1. The greatest number of formulas was detected in the 1202M sample, giving 600 more compounds than the 1203A sample, which showed the lowest number of detected compounds. This large difference in the number of compounds clearly demonstrates not only the complexity but also the variety of organic species in the aerosol samples. In addition, the number of CHON species including CHON- and CHON+ accounted for significantly higher percentages in the 1202M and 1202N samples compared to any other sample, indicating the different sources for these compound classes.

The pie charts in Figures 2 and S1 show the relative abundances (i.e., based on peak areas) of all subgroups in each sample. It was reported that the relative contributions of CHO-, CHON-, CHON+, CHOS-, and CHN+ species to wintertime OAs in urban Shanghai were close(Wang et al., 2017). However, within the present study, the relative abundances of CHON+ and CHNO- species are much greater, whereas CHOS- species represent a less fraction (Figures 2 and S1). This difference in abundances indicates that nitrogen-containing compounds, such as organonitrates, likely dominated the

physicochemical properties of aerosol particles over the MLYR channel region, whereas sulfur-containing compounds, such as organosulfates, played only a minor role compared to urban Shanghai areas.

In addition to molecular formulas, the abundances, element ratios, RDBE, the number of carbonyl group, and the values of KMD and Xc for detected species were listed in the Dataset 1. In the present study, large amounts of organics with low saturation degrees were observed in all samples. In both ESI- and ESI+, 62-72% of the determined formulas are characterized by high RDBE values (RDBE $\geq$ 4) and 39-52% of the formulas show Xc values $\geq$ 2.50, indicating that most of these compounds are aromatics (Wang et al., 2017; Yassine et al., 2014). A further analysis shows that around 15-23% of the formulas in ESI+ and 23-28% of the formulas in ESI- were probably polycyclic aromatics (Xc $\geq$ 2.71), representing more than half of the number of aromatic molecules. These results suggest that anthropogenic emissions made important contributions to the atmospheric OAs over the MLYR channel.

Li et al. (2018) classified the air pollution during the cruise campaign into eight distinct episodes based on sampling locations, backward trajectories, and photochemical processes. We note that the sampling duration for the 1201M, 1201A, and 1201N samples corresponds to episode #5 in an overview paper of the cruise campaign (Li et al., 2018), whereas that for the 1202M and 1202N samples overlaps episode #6, and the 1203A sample coincides with episode #7, respectively. Based on the concentrations of carbon monoxide, and trace elements and levoglucosan in

particulate matters, episode #5 and episodes #6-7 are cases strongly influenced by coal combustion and biomass burning, respectively (Li et al., 2018). The larger numbers and higher abundances of sulfur-containing compounds in the 1201M and 1201A samples (Figure 2 and Table 1) are probably caused by coal combustion, which is in agreement with Li et al. (2018). In addition to the most intense species detected in ESI- and ESI+ (see Figures 2 and S1, and Tables 2 and S3), other organics detected with high abundances in the samples, including C_7H_7NO, C_8H_7NO, and C_9H_7NO were assigned to the benzamide, 4-hydroxy-benzene acetonitrile, and 3-(4-hydroxyphenyl) propionitrile, respectively, which are well known tracers derived from biomass burning (Laskin et al., 2009; Lin et al., 2016; Ma & Hays, 2008). In addition to the cities and factories, there are farmland and rural areas along the Yangtze River. Compound J' (Figure 2, referred to $C_{10}H_{17}NO_7S$), with the highest abundance in the 1201M sample, is tentatively assigned to be derived from monoterpene oxidation in the presence of NO_x and SO_2 (Brüggemann et al., 2015; Seinfeld et al., 2008; Wang et al., 2018). It should be noted that these tracers may also be formed from chemical processing and cannot be distinguished in the present study, but precursor molecules with aromatic structures likely originated from the same sources. Overall, biomass burning and fossil fuel combustion could be important organic aerosol sources over the MLYR channel (Li et al., 2018).

3.2 Molecular characterization of BrC chromophores

BrC chromophores were distinguished by matching the absorption chromatograms

285 with the DAD detector to the extracted ion chromatograms. The mass spectrum before
286 and at a major absorption were compared to help identifying the potential
287 chromophores, as shown in Figure S2. We note that only chromophores with high ion
288 abundances and strong light absorptions can be unambiguously determined by this
289 approach. Indeed, the highly complex composition of the aerosol samples can lead to
290 overlapping peaks in both extracted ion chromatograms and UV-Vis absorption spectra.
291 Note that only the 1201M, 1201A and 1202N samples, which were analyzed with a
292 good DAD performance, were chosen to determine the BrC chromophore.

293 UHPLC-DAD absorption chromatograms between 290-480 nm wavelengths were
294 blank-corrected, normalized by the volume of the sample, and subsequently plotted in
295 Figures 3 and S3-S4. Intense absorption at near UV wavelengths (290-350 nm) is
296 evident. Much higher light absorption was observed in the 1202N sample than in the
297 1201M and 1201A samples, likely due to the greater concentrations of BrC
298 chromophores in the 1202N sample (Figures 2 and S1). For example, the relative
299 abundances of $C_6H_5NO_3$ in the 1201M and 1201A samples only account for around 17%
300 and 15% of that in the 1202N sample, respectively. The presence of complex mixtures
301 of chemicals including isomeric chromophores could have contributed to the humped
302 light absorption in these chromatograms (Budisulistiorini et al., 2017).

303 Following the UHPLC/DAD/HRMS protocol in Figure S2, we identified thirteen
304 BrC chromophores and their formulas were labelled next to the corresponding
305 absorption peaks in Figures 3 and S3-S4. All of them are characterized with high

unsaturation degrees (RDBE $\geqslant$ 4), indicating the presence of poly-conjugated double bonds. For example, $C_6H_5NO_3$, presumably nitrophenol, is the most abundant species in the six samples and derived from biomass burning (Mohr et al., 2013). Nitrogen-containing chromophores including $C_6H_5NO_4$, $C_7H_5NO_5$, $C_7H_7NO_3$, $C_7H_7NO_4$, $C_8H_7NO_3$, and $C_7H_6N_2O_5$ also exhibit high degrees of unsaturation and were assigned to nitro-aromatics that are also known to be emitted from biomass burning (Desyaterik et al., 2013; Lin et al., 2016). In addition to the presence of monoaromatics, products formed from the photooxidation of polycyclic aromatic hydrocarbons (PAHs) were observed (Riva et al., 2015). As an example, $C_7H_6O_2$ assigned to benzoic acid was identified in large amount in the different samples. It is worth pointing out that such carbonyl-containing compounds are well-suited candidates to act as photosensitizer, potentially inducing chemical reactions at the surface and in the bulk of aerosol particles (George et al., 2015; McNeill & Canonica, 2016). In total, more than seventy carbonyl-containing formulas were determined based on the PFBHA derivatization, with 6-24% of carbonyl-containing formulas in ESI- and 35-45% in ESI+ belonging to aromatic compounds (i.e., Xc $\geq$ 2.50, see Dataset 1). In addition, polycyclic aromatics including $C_{17}H_{10}O$ (RDBE = 13, Xc = 2.83), $C_{19}H_{10}O$ (RDBE = 15, Xc = 2.86) and $C_{13}H_8O_2$ (RDBE = 15, Xc = 2.75) were contributors to light absorption (Figures 3 and S3-S4), and the latter of which ($C_{13}H_8O_2$) is an important tracer for biomass burning (Lin et al., 2016). Finally, due to the large presence of $C_{14}H_{11}NO$ (RDBE = 10 and a Xc = 2.78; Figure S1) that is assigned to benzyloxybenzonitrile species, microorganism is another potential source of BrC compounds (Garcia-Alcega et al., 2017) within the Yangtze

River channel.

In addition to unambiguously determining the thirteen chromophores by the UHPLC/DAD/HRMS analysis, we compared the mass list of organic species in our samples and those in previously observed during biomass burning experiments (Budisulistiorini et al., 2017; Lin et al., 2016). As a result, sixty-three BrC chromophores including 31 formulas were observed only in ESI-, 14 formulas only in ESI+, and 18 formulas in both modes. The retention time of all these species corresponded to the light absorption region of the chromatogram but did not match an outstanding absorption peak. Their molecular weights are greater than 120 Da, but less than 350 Da (Figure S5) and have high RDBE values (ranging from 4 to 12), indicating that such species are likely aromatics. In addition, Figure S6 shows the distribution of the number of nitrogen (0-2) and oxygen (1-7) atoms of these seventy-six BrC chromophores. During biomass burning and fuel combustion, OH-initiated oxidation may lead to the formation of oxygenated organic compounds, producing light absorbing species (Saleh et al., 2014). Three reduced nitrogen-containing aromatic chromophores with $O/N < 3$, such as $C_{14}H_{11}NO$, were identify in ESI+, whereas more than twenty nitro-aromatic chromophores with $O/N \geq 3$ were preferably detected in ESI- (Zhang et al., 2013). These nitrogen-containing aromatics were probably produced by heterogeneous reactions of aromatics with NO_2 and nitrate radicals (NO_3) (Kwamena & Abbatt, 2008) and/or oligomerization of dicarbonyls reacting with ammonium during combustion (Budisulistiorini et al., 2017; Kampf et al., 2016).

Figures 4 and S7-S11 show the CH_2-Kendrick and Van Krevelen (VK) diagrams for the 1201M, 1201A, and 1202N samples with the seventy-six identified BrC chromophores being color-coded. Homologous compounds line up a horizontal line in the CH_2- Kendrick diagrams but a tilted one in the VK diagrams, suggesting that the homologues could have variable degrees of saturation and oxidation but possible similar structure and physicochemical properties. This leads to tentative assignments of over 120 species to BrC chromophores. These species were not outstanding either in the mass spectra or in the absorption chromatography, but could have contributed to the humped light absorption signal.

Many studies show that nitrogen-containing heterocyclic imine and imidazole compounds that are derived from reactions of carbonyls and dicarbonyls with ammonium, ammonia or amino acids, can absorb at wavelengths of 300-500 nm (De Haan et al., 2009; Kampf et al., 2016; Nguyen et al., 2013; Nozière et al., 2009; Sareen et al., 2009). For example, $C_6H_8ON_2$ could be formed from the reaction of methylglyoxal with ammonium, being an important BrC chromophore (Lin et al., 2015). However, its relative abundances only account for less than 0.6% of the most abundant ion (i.e., $C_{16}H_{33}NO$ in 1201A sample) in 1201M, 1201A and 1202N samples. In this study, 173-334 CHON+ species and 87-136 CHN+ species were determined according to their exact mass. These CHON+ compounds are characterized with low degrees of oxidation with average values of O/N lower than 1.53, indicating the presence of reduced nitrogen in the formula. In addition, 57-59% of CHON+ and 70-78% of CHN+ have high unsaturation degrees with RDBE $\geq$ 4, whereas 24-27% of CHON+ and 29-

36% of CHN+ belong to monoaromatics ($2.71 > Xc \geq 2.50$) and 6-13% of CHON+ and 34-44% of CHN+ belong to polycyclic aromatics ($Xc \geq 2.71$), respectively, suggesting that many of these reduced nitrogen-containing compounds probably contain conjugated systems and possess light absorption abilities.

3.3 Light absorption contribution of determined strong chromophores

Figure 5 shows the light absorption contribution from the 13 strong BrC chromophores unambiguously determined by UHPLC/DAD/HRMS to the total light absorption of OAs at 290-480 nm. The light absorption for each chromophore was summed up based on the corresponding ion chromatogram.

Overall, the total light absorption of OAs is the highest for the 1202N sample and the lowest for the 1201A samples. The maximum absorption was observed at 290 nm, and the total absorption decreased as the wavelength increased, showing a similar trend to that in the study of Lin et al. (2016). However, in this study, the light absorptions are almost zero at wavelength of 400 nm, and thus, lower than those of the study of Lin et al. (2016). This weakened absorption probably indicates larger concentrations of chromophores in biomass burning aerosols collected in their study compared to the ambient aerosol samples collected over the MLYR channel. At 290 nm, around 35-37% of the light absorption of OAs can be attributed to the 13 strong BrC chromophores, whose contribution increased to around 58-70% at 350 nm. In particular, the determined nitro-aromatics (i.e., $C_6H_5NO_3$, $C_6H_5NO_4$, $C_7H_7NO_3$, $C_7H_7NO_4$, $C_7H_5NO_5$, $C_8H_7NO_3$, $C_8H_9NO_3$, and $C_7H_6N_2O_5$) alone contribute to about 25-27% at 290 nm and 55-65% at

350 nm of the total light absorption of OAs. Moreover, it should be noted that the light absorption of the chromophores from biomass burning (i.e., $C_6H_5NO_3$, $C_6H_5NO_4$, $C_7H_5NO_5$, $C_7H_7NO_3$, $C_7H_7NO_4$, $C_8H_7NO_3$, $C_7H_6N_2O_5$, and $C_{13}H_8O_2$) account for 27-28% at 290 nm and 55-68% at 350 nm, further indicating that biomass burning is potentially the most important sources for light-absorbing species in aerosol particles in the MLYR region.

4. Conclusions

Nearly one-third of the Chinese population live along the Yangtze River; the air pollution over the MLYR channel region can impact the aquatic ecosystem, the health of local residents, and regional climate. Therefore, it becomes crucial to characterize the constituents and sources of air pollutants over the MLYR channel region. To the best of our knowledge, YRC is the first comprehensive cruise observation of air quality along the MLYR channel. The chemical composition of the organic fraction of atmospheric particles over this region was investigated, for the first time, using UHPLC/DAD/HRMS with a special focus on BrC chromophores in the present study, which will significantly improve our understanding of BrC compositions, sources and optical properties in this region. So far, only a few studies have investigated atmospheric BrC at such a detailed molecular level. In total, 695-1187 and 450-695 molecular formulas were determined in ESI- and ESI+, respectively. In addition, 62-72% of the organic compounds exhibit high degrees of unsaturation (RDBE $\geq$ 4). Furthermore, 39-52% and 15-23% of these organics have an Xc $\geq$ 2.50 and Xc $\geq$ 2.71,

indicating that they are aromatics and polycyclic aromatics, respectively. Moreover, high signal abundances and large numbers of known tracers indicate that biomass burning and fossil fuel combustion are important sources for OAs in the MLYR region.

In total, thirteen strong chromophores were determined by UHPLC/DAD/HRMS analysis. Most of these compounds are probably derived from biomass burning. Apart from that, more than sixty chromophores identified in previous biomass burning experiments were also detected in this study, further confirming the abundance of biomass burning emissions in the MLYR. All of these chromophores were characterized by a low degree of saturation, and Xc values indicating aromatic, nitro-aromatic, and polycyclic aromatic structures. Based on KMD and VK analyses, around one hundred homologues to the identified chromophores were detected, probably having similar structures and light-absorption properties. A large amount of reduced nitrogen-containing compounds and potential photosensitizers (i.e., carbonyl-containing compounds) were found, probably contributing further to the light absorptions of aerosols in the MLYR.

We found that the determined thirteen strong chromophores contribute to around 35-37% at 290 nm and 58-70% at 350 nm of the overall light absorption of OAs, respectively. The light absorption contributions of chromophores from biomass burning were estimated to 27-28% at 290 nm and 55-68% at 350 nm, highlighting the importance of such anthropogenic emissions for light-absorption properties of aerosol particles over the MLYR channel region.

Acknowledgments

This study was financially supported by the National Natural Science Foundation of China (91644213, 21925601 and 41575113), the National Key R&D Program of China (2017YFC0209505), the ANR-RGC Programme (project ANR-16-CE01-0013), the European Union's Horizon 2020 research and innovation program under grant agreement No. 690958 (MARSU). The authors declare no competing interests. All data to support the conclusions of this manuscript are included in the main text and supplementary materials, or data could be download at https://nuage.catalyse.cnrs.fr/s/mj7gwfQXpdWnAEL.

References:

Andreae, M O, & Gelencsér, A. (2006). Atmospheric Chemistry and Physics Black carbon or brown carbon? The nature of light-absorbing carbonaceous aerosols. *Atmos. Chem. Phys*, *6*, 3131–3148. Retrieved from www.atmos-chem-phys.net/6/3131/2006/

Andreae, Meinrat O., & Crutzen, P. J. (1997). Atmospheric aerosols: Biogeochemical sources and role in atmospheric chemistry. *Science*, *276*(5315), 1052–1058. https://doi.org/10.1126/science.276.5315.1052

Bahadur, R., Praveen, P. S., Xu, Y., & Ramanathan, V. (2012). Solar absorption by elemental and brown carbon determined from spectral observations. *Proceedings of the National Academy of Sciences*, *109*(43), 17366–17371. https://doi.org/10.1073/pnas.1205910109

Bones, D. L., Henricksen, D. K., Mang, S. A., Gonsior, M., Bateman, A. P., Nguyen, T. B., et al. (2010). Appearance of strong absorbers and fluorophores in limonene-O<inf>3</inf> secondary organic aerosol due to NH<inf>4</inf>$^{+}$ -mediated chemical aging over long time scales. *Journal of Geophysical Research Atmospheres*, *115*(5), 1–14. https://doi.org/10.1029/2009JD012864

Borrás, E., & Tortajada-Genaro, L. A. (2012). Determination of oxygenated compounds in secondary organic aerosol from isoprene and toluene smog chamber experiments. *International Journal of Environmental Analytical Chemistry*, *92*(1), 110–124. https://doi.org/10.1080/03067319.2011.572164

Brüggemann, M., Karu, E., Stelzer, T., & Hoffmann, T. (2015). Real-time analysis of ambient organic aerosols using aerosol flowing atmospheric-pressure afterglow mass spectrometry (AeroFAPA-MS). *Environmental Science and Technology*, *49*(9), 5571–5578. https://doi.org/10.1021/es506186c

Budisulistiorini, S. H., Riva, M., Williams, M., Chen, J., Itoh, M., Surratt, J. D., & Kuwata, M. (2017). Light-Absorbing Brown Carbon Aerosol Constituents from Combustion of Indonesian Peat and Biomass. *Environmental Science and Technology*, *51*(8), 4415–4423. https://doi.org/10.1021/acs.est.7b00397

Chakrabarty, R. K., Moosmüller, H., Chen, L. W. A., Lewis, K., Arnott, W. P., Mazzoleni, C., et al. (2010).

Brown carbon in tar balls from smoldering biomass combustion. *Atmospheric Chemistry and Physics*, *10*(13), 6363–6370. https://doi.org/10.5194/acp-10-6363-2010

Chung, C. E., Ramanathan, V., & Decremer, D. (2012). Observationally constrained estimates of carbonaceous aerosol radiative forcing. *Proceedings of the National Academy of Sciences*, *109*(29), 11624–11629. https://doi.org/10.1073/pnas.1203707109

Desyaterik, Y., Sun, Y., Shen, X., Lee, T., Wang, X., Wang, T., & Collett, J. L. (2013). Speciation of "brown" carbon in cloud water impacted by agricultural biomass burning in eastern China. *Journal of Geophysical Research Atmospheres*, *118*(13), 7389–7399. https://doi.org/10.1002/jgrd.50561

Feng, Y., Ramanathan, V., & Kotamarthi, V. R. (2013). Brown carbon: A significant atmospheric absorber of solar radiation. *Atmospheric Chemistry and Physics*, *13*(17), 8607–8621. https://doi.org/10.5194/acp-13-8607-2013

Fleming, L. T., Lin, P., Laskin, A., Laskin, J., Weltman, R., Edwards, R. D., et al. (2018). Molecular composition of particulate matter emissions from dung and brushwood burning household cookstoves in Haryana, India. *Atmos. Chem. Phys*, *185194*, 2461–2480. https://doi.org/10.5194/acp-18-2461-2018

Garcia-Alcega, S., Nasir, Z. A., Ferguson, R., Whitby, C., Dumbrell, A. J., Colbeck, I., et al. (2017). Fingerprinting outdoor air environment using microbial volatile organic compounds (MVOCs) – A review. *TrAC - Trends in Analytical Chemistry*, *86*, 75–83. https://doi.org/10.1016/j.trac.2016.10.010

George, C., Ammann, M., D'Anna, B., Donaldson, D. J., & Nizkorodov, S. A. (2015). Heterogeneous Photochemistry in the Atmosphere. *Chemical Reviews*, *115*(10), 4218–4258. https://doi.org/10.1021/cr500648z

Goldstein, A. H., & Galbally, I. E. (2007). Known and Unexplored ORGANIC CONSTITUENTS in the Earth's Atmosphere Much remains to be learned about the sources, structure, chemistry, and fate of gas-phase and aerosol organic compounds. *Environmental Science & Technology*, (1), 1515–1521.

Gómez-González, Y., Wang, W., Vermeylen, R., Chi, X., Neirynck, J., Janssens, I. A., et al. (2012). Chemical characterisation of atmospheric aerosols during a 2007 summer field campaign at Brasschaat, Belgium: Sources and source processes of biogenic secondary organic aerosol. *Atmospheric Chemistry and Physics*, *12*(1), 125–138. https://doi.org/10.5194/acp-12-125-2012

De Haan, D. O., Tolbert, M. A., & Jimenez, J. L. (2009). Atmospheric condensed-phase reactions of glyoxal with methylamine. *Geophysical Research Letters*, *36*(11), 2–6. https://doi.org/10.1029/2009GL037441

Huang, C., Chen, C. H., Li, L., Cheng, Z., Wang, H. L., Huang, H. Y., et al. (2011). Emission inventory of anthropogenic air pollutants and VOC species in the Yangtze River Delta region, China. *Atmospheric Chemistry and Physics*, *11*(9), 4105–4120. https://doi.org/10.5194/acp-11-4105-2011

Hughey, C. A., Hendrickson, C. L., Rodgers, R. P., Marshall, A. G., & Qian, K. (2001). Kendrick Mass Defect Spectrum: A Compact Visual Analysis for Ultrahigh-Resolution Broadband Mass Spectra. *Analytical Chemistry*, *73*(19), 4676–4681. https://doi.org/10.1021/ac010560w

Iinuma, Y., Brüggemann, E., Gnauk, T., Müller, K., Andreae, M. O., Helas, G., et al. (2007). Source characterization of biomass burning particles: The combustion of selected European conifers, African hardwood, savanna grass, and German and Indonesian peat. *Journal of Geophysical Research Atmospheres*, *112*(8). https://doi.org/10.1029/2006JD007120

Iinuma, Yoshiteru, Böge, O., & Herrmann, H. (2010). Methyl-nitrocatechols: Atmospheric tracer

compounds for biomass burning secondary organic aerosols. *Environmental Science and Technology*, *44*(22), 8453–8459. https://doi.org/10.1021/es102938a

Ito, T., Bekki, K., Fujitani, Y., & Hirano, S. (2019). The toxicological analysis of secondary organic aerosol in human lung epithelial cells and macrophages, 22747–22755.

Jacobson, M. Z. (2001). Strong radiative heating due to the mixing state of black carbon in atmospheric aerosols. *Nature*, *409*(6821), 695–697. https://doi.org/10.1038/35055518

Jang, M., & Kamens, R. M. (2001). Characterization of secondary aerosol from the photooxidation of toluene in the presence of NOx and 1-propene. *Environmental Science and Technology*, *35*(18), 3626–3639. https://doi.org/10.1021/es010676+

Kampf, C. J., Filippi, A., Zuth, C., Hoffmann, T., & Opatz, T. (2016). Secondary brown carbon formation: Via the dicarbonyl imine pathway: Nitrogen heterocycle formation and synergistic effects. *Physical Chemistry Chemical Physics*, *18*(27), 18353–18364. https://doi.org/10.1039/c6cp03029g

Kanakidou, M., Seinfeld, J. H., Pandis, S. N., Barnes, I., Dentener, F. J., Facchini, M. C., et al. (2005). Organic aerosol and global climate modelling: a review. *Atmospheric Chemistry and Physics*, *5*(4), 1053–1123. https://doi.org/10.5194/acp-5-1053-2005

Kuang, B. Y., Yeung, H. S., Lee, C. C., Griffith, S. M., & Yu, J. Z. (2018). Aromatic formulas in ambient PM2.5 samples from Hong Kong determined using FT-ICR ultrahigh-resolution mass spectrometry. *Analytical and Bioanalytical Chemistry*, *410*(24), 6289–6304. https://doi.org/10.1007/s00216-018-1239-8

Kuhl, C., Tautenhahn, R., Böttcher, C., Larson, T. R., & Neumann, S. (2012). CAMERA: An integrated strategy for compound spectra extraction and annotation of liquid chromatography/mass spectrometry data sets. *Analytical Chemistry*, *84*(1), 283–289. https://doi.org/10.1021/ac202450g

Kwamena, N. O. A., & Abbatt, J. P. D. (2008). Heterogeneous nitration reactions of polycyclic aromatic hydrocarbons and n-hexane soot by exposure to NO3/NO2/N2O5. *Atmospheric Environment*, *42*(35), 8309–8314. https://doi.org/10.1016/j.atmosenv.2008.07.037

Lambe, a T., Cappa, C. D., Massoli, P., Onasch, T. B., Forestieri, S. D., Martin, a T., & Cummings, M. J. (2012). Relationship between oxidation level and optical properties of secondary organic aerosol α -pinene naphthalene guaiacol JP-10, 2467.

Laskin, A., Smith, J. S., & Laskin, J. (2009). Molecular Characterization of Nitrogen-Containing Organic Compounds in Biomass Burning Aerosols Using High-Resolution Mass Spectrometry. *Environmental Science & Technology*, *43*(10), 3764–3771. https://doi.org/10.1021/es803456n

Laskin, A., Laskin, J., & Nizkorodov, S. A. (2015). Chemistry of Atmospheric Brown Carbon. *Chemical Reviews*, *115*(10), 4335–4382. https://doi.org/10.1021/cr5006167

Lee, A. K. Y., Zhao, R., Li, R., Liggio, J., Li, S. M., & Abbatt, J. P. D. (2013). Formation of light absorbing organo-nitrogen species from evaporation of droplets containing glyoxal and ammonium sulfate. *Environmental Science and Technology*, *47*(22), 12819–12826. https://doi.org/10.1021/es402687w

Lee, H. J., Aiona, P. K., Laskin, A., Laskin, J., & Nizkorodov, S. A. (2014). Effect of solar radiation on the optical properties and molecular composition of laboratory proxies of atmospheric brown carbon. *Environmental Science and Technology*, *48*(17), 10217–10226. https://doi.org/10.1021/es502515r

Lei, T., Zuend, A., Wang, W. G., Zhang, Y. H., & Ge, M. F. (2014). Hygroscopicity of organic compounds from biomass burning and their influence on the water uptake of mixed organic ammonium sulfate aerosols. *Atmospheric Chemistry and Physics*, *14*(20), 11165–11183. https://doi.org/10.5194/acp-14-11165-2014

Li, Z., Li, C., Ye, X., Fu, H., Wang, L., Yang, X., et al. (2018). Air quality in the middle and lower reaches of the Yangtze River channel: A cruise campaign. *Atmospheric Chemistry and Physics*, *18*(19), 14445–14464. https://doi.org/10.5194/acp-18-14445-2018

Lin, G., Penner, J. E., Flanner, M. G., Sillman, S., Xu, L., & Zhou, C. (2014). Radiative forcing of organic aerosol in the atmosphere and on snow: Effects of SOA and brown carbon. *Journal of Geophysical Research*, *119*(12), 7453–7476. https://doi.org/10.1002/2013JD021186

Lin, P., Rincon, A. G., Kalberer, M., & Yu, J. Z. (2012). Elemental composition of HULIS in the Pearl River Delta Region, China: Results inferred from positive and negative electrospray high resolution mass spectrometric data. *Environmental Science and Technology*, *46*(14), 7454–7462. https://doi.org/10.1021/es300285d

Lin, P., Laskin, J., Nizkorodov, S. A., & Laskin, A. (2015). Revealing Brown Carbon Chromophores Produced in Reactions of Methylglyoxal with Ammonium Sulfate. *Environmental Science and Technology*, *49*(24), 14257–14266. https://doi.org/10.1021/acs.est.5b03608

Lin, P., Aiona, P. K., Li, Y., Shiraiwa, M., Laskin, J., Nizkorodov, S. A., & Laskin, A. (2016). Molecular Characterization of Brown Carbon in Biomass Burning Aerosol Particles. *Environmental Science and Technology*, *50*(21), 11815–11824. https://doi.org/10.1021/acs.est.6b03024

Lin, P., Fleming, L. T., Nizkorodov, S. A., Laskin, J., & Laskin, A. (2018). Comprehensive Molecular Characterization of Atmospheric Brown Carbon by High Resolution Mass Spectrometry with Electrospray and Atmospheric Pressure Photoionization. *Analytical Chemistry*, *90*(21), 12493–12502. https://doi.org/10.1021/acs.analchem.8b02177

Lin, Y. H., Budisulistiorini, S. H., Chu, K., Siejack, R. A., Zhang, H. F., Riva, M., et al. (2014). Light-absorbing oligomer formation in secondary organic aerosol from reactive uptake of isoprene epoxydiols. *Environmental Science and Technology*, *48*(20), 12012–12021. https://doi.org/10.1021/es503142b

Ma, Y., & Hays, M. D. (2008). Thermal extraction-two-dimensional gas chromatography-mass spectrometry with heart-cutting for nitrogen heterocyclics in biomass burning aerosols. *Journal of Chromatography A*, *1200*(2), 228–234. https://doi.org/10.1016/j.chroma.2008.05.078

McNeill, K., & Canonica, S. (2016). Triplet state dissolved organic matter in aquatic photochemistry: Reaction mechanisms, substrate scope, and photophysical properties. *Environmental Science: Processes and Impacts*, *18*(11), 1381–1399. https://doi.org/10.1039/c6em00408c

Mohr, C., Lopez-Hilfiker, F. D., Zotter, P., Prévoît, A. S. H., Xu, L., Ng, N. L., et al. (2013). Contribution of nitrated phenols to wood burning brown carbon light absorption in detling, united kingdom during winter time. *Environmental Science and Technology*, *47*(12), 6316–6324. https://doi.org/10.1021/es400683v

Nguyen, T. B., Lee, P. B., Updyke, K. M., Bones, D. L., Laskin, J., Laskin, A., & Nizkorodov, S. A. (2012). Formation of nitrogen- and sulfur-containing light-absorbing compounds accelerated by evaporation of water from secondary organic aerosols. *Journal of Geophysical Research Atmospheres*, *117*(1), 1–14. https://doi.org/10.1029/2011JD016944

Nguyen, T. B., Laskin, A., Laskin, J., & Nizkorodov, S. A. (2013). Brown carbon formation from ketoaldehydes of biogenic monoterpenes. *Faraday Discussions*, *165*, 473–494. https://doi.org/10.1039/c3fd00036b

Nozière, B., Dziedzic, P., & Córdova, A. (2009). Products and kinetics of the liquid-phase reaction of glyoxal catalyzed by ammonium ions (NH4+). *Journal of Physical Chemistry A*, *113*(1), 231–237. https://doi.org/10.1021/jp8078293

Pöschl, U. (2005). Atmospheric aerosols: Composition, transformation, climate and health effects. *Angewandte Chemie - International Edition*, *44*(46), 7520–7540. https://doi.org/10.1002/anie.200501122

Rincón, A. G., Guzmán, M. I., Hoffmann, M. R., & Colussi, A. J. (2010). Thermochromism of model organic aerosol matter. *Journal of Physical Chemistry Letters*, *1*(1), 368–373. https://doi.org/10.1021/jz900186e

Riva, M., Robinson, E. S., Perraudin, E., Donahue, N. M., & Villenave, E. (2015). Photochemical aging of secondary organic aerosols generated from the photooxidation of polycyclic aromatic hydrocarbons in the gas-phase. *Environmental Science and Technology*, *49*(9), 5407–5416. https://doi.org/10.1021/acs.est.5b00442

Saleh, R., Robinson, E. S., Tkacik, D. S., Ahern, A. T., Liu, S., Aiken, A. C., et al. (2014). Brownness of organics in aerosols from biomass burning linked to their black carbon content. *Nature Geoscience*, *7*(9), 647–650. https://doi.org/10.1038/ngeo2220

Sareen, N., Shapiro, E. L., Schwier, A. N., & McNeill, V. F. (2009). Secondary organic material formed by methylglyoxal in aqueous aerosol mimics – Part 2: Product identification using Aerosol-CIMS. *Atmospheric Chemistry and Physics Discussions*, *9*(4), 15567–15594. https://doi.org/10.5194/acpd-9-15567-2009

Seinfeld, J. H., Surratt, J. D., Gomez-Gonzalez, Y., Chan, A. W. H., Vermeylen, R., Shahgholi, M., et al. (2008). Organosulfate formation in biogenic secondary organic aerosol. *Journal of Physical Chemistry A*, *112*(36), 8345–8378. https://doi.org/Doi 10.1021/Jp802310p

Shapiro, E. L., Szprengiel, J., Sareen, N., Jen, C. N., Giordano, M. R., & McNeill, V. F. (2009). Light-absorbing secondary organic material formed by glyoxal in aqueous aerosol mimics. *Atmospheric Chemistry and Physics*, *9*(7), 2289–2300. https://doi.org/10.5194/acp-9-2289-2009

Tang, M., Alexander, J. M., Kwon, D., Estillore, A. D., Laskina, O., Young, M. A., et al. (2016). Optical and Physicochemical Properties of Brown Carbon Aerosol: Light Scattering, FTIR Extinction Spectroscopy, and Hygroscopic Growth. *Journal of Physical Chemistry A*, *120*(24), 4155–4166. https://doi.org/10.1021/acs.jpca.6b03425

Wang, X., Hayeck, N., Brüggemann, M., Yao, L., Chen, H., Zhang, C., et al. (2017). Chemical Characteristics of Organic Aerosols in Shanghai: A Study by Ultra-High-Performance Liquid Chromatography Coupled with Orbitrap Mass Spectrometry. *Journal of Geophysical Research: Atmospheres*, 1–20. https://doi.org/10.1002/2017JD026930

Wang, X. K., Rossignol, S., Ma, Y., Yao, L., Wang, M. Y., Chen, J. M., et al. (2016). Molecular characterization of atmospheric particulate organosulfates in three megacities at the middle and lower reaches of the Yangtze River. *Atmospheric Chemistry and Physics*, *16*(4), 2285–2298. https://doi.org/10.5194/acp-16-2285-2016

Wang, Y., Hu, M., Lin, P., Guo, Q., Wu, Z., Li, M., et al. (2017). Molecular Characterization of Nitrogen-Containing Organic Compounds in Humic-like Substances Emitted from Straw Residue Burning. *Environmental Science and Technology*, *51*(11), 5951–5961. https://doi.org/10.1021/acs.est.7b00248

Wang, Y., Hu, M., Guo, S., Wang, Y., Zheng, J., Yang, Y., et al. (2018). The secondary formation of organosulfates under interactions between biogenic emissions and anthropogenic pollutants in summer in Beijing. *Atmospheric Chemistry and Physics*, *18*(14), 10693–10713. https://doi.org/10.5194/acp-18-10693-2018

Yang, M., Howell, S. G., Zhuang, J., & Huebert, B. J. (2009). Attribution of aerosol light absorption to

black carbon, brown carbon, and dust in China - Interpretations of atmospheric measurements during EAST-AIRE. *Atmospheric Chemistry and Physics*, *9*(6), 2035–2050. https://doi.org/10.5194/acp-9-2035-2009

Yassine, M. M., Harir, M., Dabek-Zlotorzynska, E., & Schmitt-Kopplin, P. (2014). Structural characterization of organic aerosol using Fourier transform ion cyclotron resonance mass spectrometry: aromaticity equivalent approach. *Rapid Communications in Mass Spectrometry : RCM*, *28*(22), 2445–2454. https://doi.org/10.1002/rcm.7038

Zhang, X., Lin, Y. H., Surratt, J. D., & Weber, R. J. (2013). Sources, composition and absorption Ångström exponent of light-absorbing organic components in aerosol extracts from the los angeles basin. *Environmental Science and Technology*, *47*(8), 3685–3693. https://doi.org/10.1021/es305047b

Zhao, R., Lee, A. K. Y., Huang, L., Li, X., Yang, F., & Abbatt, J. P. D. (2015). Photochemical processing of aqueous atmospheric brown carbon. *Atmospheric Chemistry and Physics*, *15*(11), 6087–6100. https://doi.org/10.5194/acp-15-6087-2015

Supporting References:

Brüggemann, M., Hayeck, N., Bonnineau, C., Pesce, S., Alpert, P. A., Perrier, S., et al. (2017). Interfacial photochemistry of biogenic surfactants: A major source of abiotic volatile organic compounds. *Faraday Discussions*, *200*, 59–74. https://doi.org/10.1039/c7fd00022g

Cheng, Y., Fai Ho, K., Jing Wu, W., Hang Ho, S. S., Cheng Lee, S., Huang, Y., et al. (2012). Real-time characterization of particle-bound polycyclic aromatic hydrocarbons at a heavily trafficked roadside site. *Aerosol and Air Quality Research*, *12*(6), 1181–1188. https://doi.org/10.4209/aaqr.2011.11.0223

Fleming, L. T., Lin, P., Laskin, A., Laskin, J., Weltman, R., Edwards, R. D., et al. (2018). Molecular composition of particulate matter emissions from dung and brushwood burning household cookstoves in Haryana, India. *Atmos. Chem. Phys*, *185194*, 2461–2480. https://doi.org/10.5194/acp-18-2461-2018

Garcia-Alcega, S., Nasir, Z. A., Ferguson, R., Whitby, C., Dumbrell, A. J., Colbeck, I., et al. (2017). Fingerprinting outdoor air environment using microbial volatile organic compounds (MVOCs) – A review. *TrAC - Trends in Analytical Chemistry*, *86*, 75–83. https://doi.org/10.1016/j.trac.2016.10.010

Ge, X., Wexler, A. S., & Clegg, S. L. (2011). Atmospheric amines - Part I. A review. *Atmospheric Environment*, *45*(3), 524–546. https://doi.org/10.1016/j.atmosenv.2010.10.012

Riva, M., Robinson, E. S., Perraudin, E., Donahue, N. M., & Villenave, E. (2015). Photochemical aging of secondary organic aerosols generated from the photooxidation of polycyclic aromatic hydrocarbons in the gas-phase. *Environmental Science and Technology*, *49*(9), 5407–5416. https://doi.org/10.1021/acs.est.5b00442

Teich, M., Van Pinxteren, D., Kecorius, S., Wang, Z., & Herrmann, H. (2016). First Quantification of Imidazoles in Ambient Aerosol Particles: Potential Photosensitizers, Brown Carbon Constituents, and Hazardous Components. *Environmental Science and Technology*, *50*(3), 1166–1173. https://doi.org/10.1021/acs.est.5b05474

Wang, X., Hayeck, N., Brüggemann, M., Yao, L., Chen, H., Zhang, C., et al. (2017). Chemical Characteristics of Organic Aerosols in Shanghai: A Study by Ultra-High-Performance Liquid Chromatography Coupled with Orbitrap Mass Spectrometry. *Journal of Geophysical Research:*

Atmospheres, 1–20. https://doi.org/10.1002/2017JD026930

Yang, H., Mei, L., Wang, P., Genereux, J., Wang, Y., Yi, B., et al. (2017). Photocatalytic degradation of norfloxacin on different TiO_{2-X} polymorphs under visible light in water. *RSC Adv.*, *7*(72), 45721–45732. https://doi.org/10.1039/C7RA09022F

Yassine, M. M., Harir, M., Dabek-Zlotorzynska, E., & Schmitt-Kopplin, P. (2014). Structural characterization of organic aerosol using Fourier transform ion cyclotron resonance mass spectrometry: aromaticity equivalent approach. *Rapid Communications in Mass Spectrometry : RCM*, *28*(22), 2445–2454. https://doi.org/10.1002/rcm.7038

Table 1. Summary of the sampling location, sampling time, and the number of assigned formulas in both ESI- and ESI+ mass spectra.

Sample ID	Time	Start point	End point	Number of Formulas (Fraction %)								
				CHO-	CHON-	CHOS-	CHONS-	All in ESI-	CHO+	CHON+	CHN+	All in ESI+
1201M	1 Dec, 2015, 7:30 am -12:00 am	(30.10°N, 115.32°E)	(29.82°N, 115.73°E)	261 (26.2%)	238 (23.9%)	253 (25.4%)	243 (24.4%)	995 (100%)	209 (41.7%)	202 (40.3%)	90 (18.0%)	501 (100%)
1201A	1 Dec, 2015, 12:00 am -6:00 pm	(29.82°N, 115.73°E)	(29.90°N, 116.48°E)	251 (26.2%)	259 (27.0%)	241 (25.1%)	208 (21.7%)	959 (100%)	190 (42.2%)	173 (38.4%)	87 (19.3%)	450 (100%)
1201N	1 Dec, 2015, 6:00 pm -12:00 pm	(29.90°N, 116.48°E)	(30.37°N, 116.89°E)	295 (26.5%)	323 (29.0%)	253 (22.7%)	242 (21.7%)	1113 (100%)	232 (38.0%)	246 (40.3%)	133 (21.8%)	611 (100%)
1202M	2 Dec, 2015, 6:00 am -12:00 am	(30.63°N, 117.24°E)	(31.10°N, 117.76°E)	291 (24.5%)	367 (30.9%)	258 (21.7%)	271 (22.8%)	1187 (100%)	235 (36.6%)	269 (41.8%)	139 (21.6%)	643 (100%)
1202N	2 Dec, 2015, 6:00 pm -12:00 pm	(31.42°N, 118.35°E)	(32.05°N, 118.69°E)	289 (26.1%)	353 (31.9%)	222 (20.0%)	244 (22.0%)	1108 (100%)	225 (32.4%)	334 (48.1%)	136 (19.6%)	695 (100%)
1203A	3 Dec, 2015, 12:00 am -6:00 pm	(32.22°N, 119.21°E)	(32.21°N, 119.55°E)	201 (28.9%)	209 (30.1%)	155 (22.3%)	130 (18.7%)	695 (100%)	209 (40.5%)	191 (37.0%)	116 (22.5%)	516 (100%)

713 Table 2. Potential identities and sources for the most abundant species in the ESI- mass spectra.

ID	Retention Time (min）	Neutral Mass (Da)	Formula	RDBE[a]	Xc[b]	Potential Identity	Potential Source/ Precursor	Reference
A’	6.09; 6.67;7.21	122.0366	$C_7H_6O_2$	5	2.50	Benzoic acid	Naphthalene	(Riva et al., 2015)
B’	8.56	139.0268	$C_6H_5NO_3$	5	2.50	Nitrophenol	Biomass burning	(Mohr et al., 2013)
C’	9.15; 9.42	153.0424	$C_7H_7NO_3$	5	2.50	Methyl nitrophenol	Biomass burning	(Mohr et al., 2013)
D’	7.73; 8.57	155.0217	$C_6H_5NO_4$	5	2.33	Nitrocatechols	Biomass burning and vehicle emissions	(Mohr et al., 2013)
E’	6.02; 7.60; 9.15; 9.53	165.0553	$C_8H_7NO_3$	6	2.60	Nitroacetophenone	Biomass burning	(Lin et al., 2016)
F’	6.10; 6.67; 6.76	166.0264	$C_8H_6O_4$	6	2.50	Phthalic acid	Naphthalene	(Riva et al., 2015)
G’	7.39; 8.32; 8.58; 8.70; 8.82; 9.47	169.0473	$C_7H_7NO_4$	5	2.33	Methyl nitrocatechols	Biomass burning and diesel exhaust	(Yoshiteru Iinuma et al., 2010)
H’	7.84; 8.10; 9.01; 9.34; 9.55; 10.15	183.0699	$C_8H_9NO_4$	5	2.33	Dimethoxynitrobenzene	Biomass burning	(Desyaterik et al., 2013)
I’	9.80; 9.96; 10.42	198.0492	$C_7H_6N_2O_5$	6	2.50	Methyl dinitrophenol	Toluene; biomass burning	(Jang & Kamens, 2001; Desyaterik et al., 2013)
J’	8.33; 8.61; 8.79; 8.91	295.0721	$C_{10}H_{17}NO_7S$	3	0	A nitrooxy organosulfate	α-pinene; β-pinene; α-terpinene; Terpinolene	(Gómez-González et al., 2012)

714 [a]Ring and double bond number. [b]Aromaticity equivalents.

Figure Captions

Figure 1. The start and end points for the filter sampling along the Yangtze River channel.

Figure 2. Mass spectra of detected CHO-, CHOS-, CHON-, and CHONS- compounds, reconstructed from extracted ion chromatograms (UHPLC-Orbitrap MS analysis, ESI-). Note that the abundance of $C_6H_5NO_3$ in the 1202N sample (the most abundant one in all samples) was set arbitrarily to 100%. The sizes of pie charts are proportional to the total abundance of all subgroups in each sample.

Figure 3. UHPLC-DAD absorption chromatograms for the 1202N aerosol sample. Panel (a) shows the blank-subtracted absorption chromatograms at two selected wavelengths (i.e., 300 and 350 nm). Panel (b) shows the blank-subtracted absorption chromatograms at 290-480 nm. The absorption peaks are labeled with the most likely formula of the light-absorbing chromophore. Molecular formulas in red, blue, and black colors represent detection in ESI-, ESI+, and both modes, respectively.

Figure 4. (a-b) CH_2-Kendrick diagrams and (c-d) Van Krevelen diagrams for CHO- and CHON- species in the 1202N aerosol sample, respectively. Purple and orange points denote the light-absorbing CHO- and CHON- compounds, respectively. The size of the points corresponds to the abundance of the corresponding ion signal.

Figure 5. Relative contribution of the thirteen BrC chromophores to the total light absorption of OAs for the (a) 1201M, (b) 1201A, and (c) 1202N samples. Note that the light-absorption at 290 nm in the 1202N sample (the highest light absorption signal in all samples) was set arbitrarily to 100%.

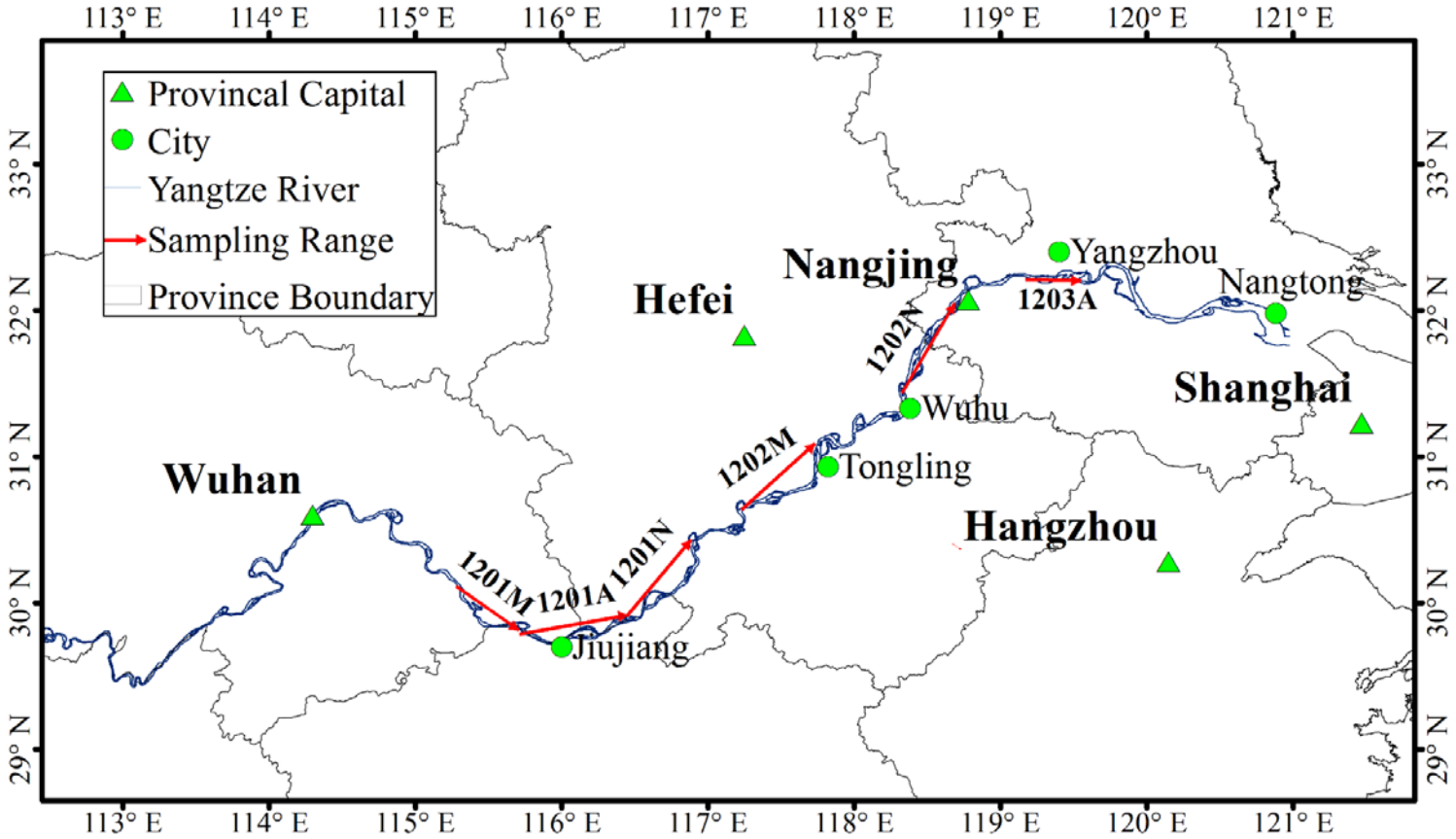

741
742 **Figure 1**
743

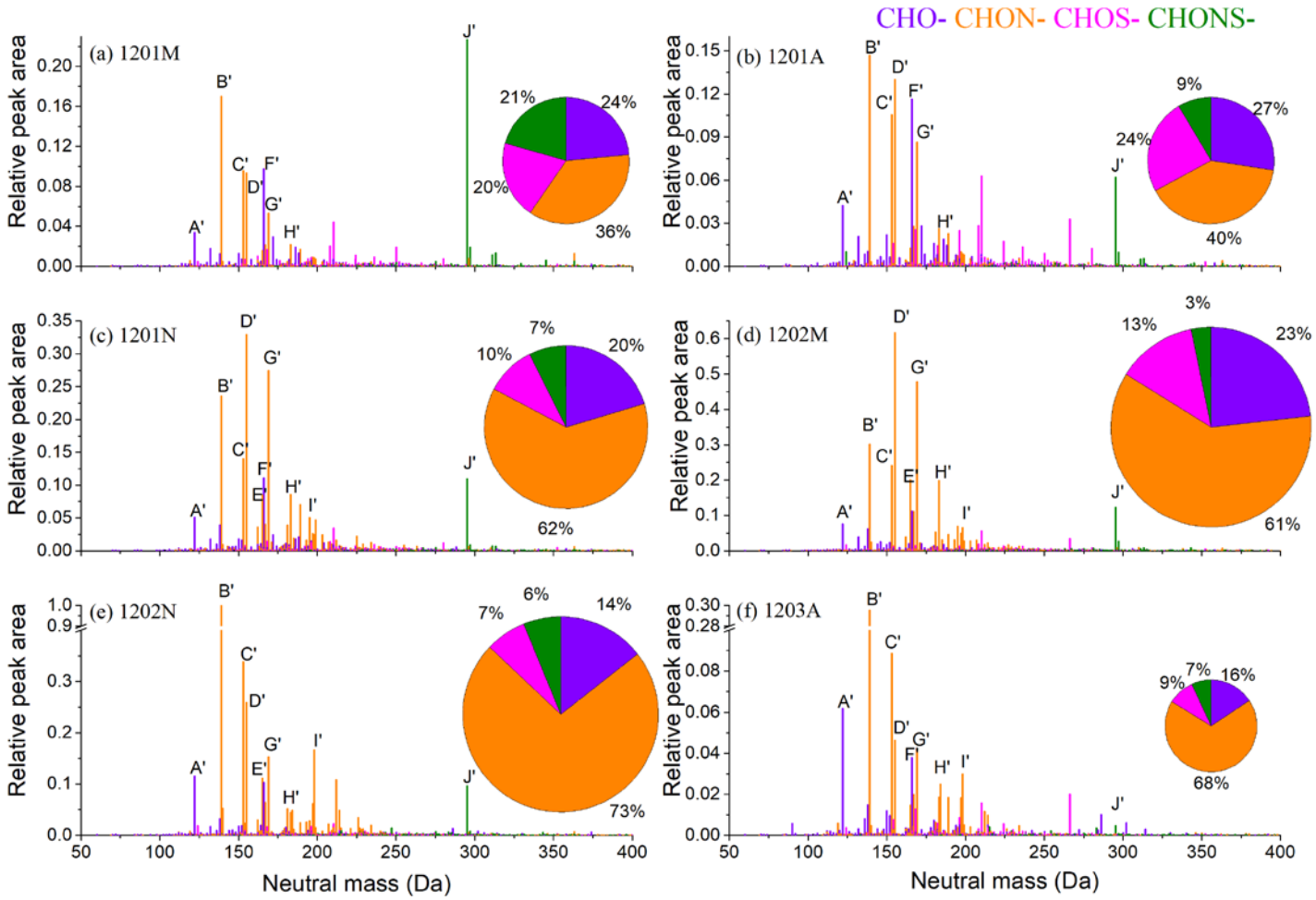

744
745

Figure 2

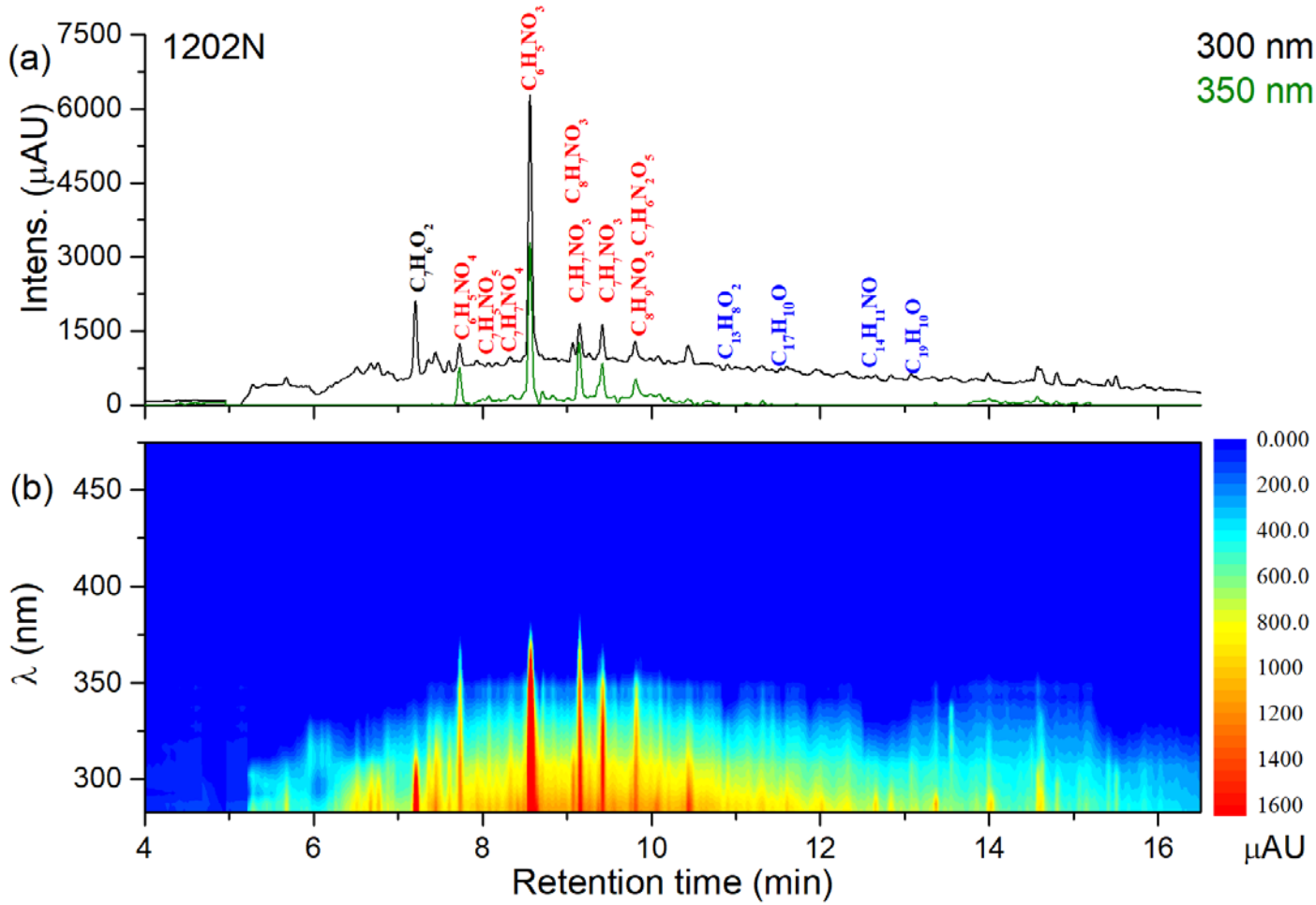
(a)
1202N
300 nm
350 nm
Intens. (μAU)
7500
6000
4500
3000
1500
0
$C_7H_6O_2$
$C_6H_5NO_4$
$C_7H_5NO_5$
$C_7H_7NO_4$
$C_6H_5NO_3$
$C_7H_7NO_3$
$C_8H_7NO_3$
$C_7H_7NO_3$
$C_8H_9NO_3$ $C_7H_6N_2O_5$
$C_{13}H_8O_2$
$C_{17}H_{10}O$
$C_{14}H_{11}NO$
$C_{19}H_{10}O$
(b)
λ (nm)
450
400
350
300
4
6
8
10
12
14
16
Retention time (min)
0.000
200.0
400.0
600.0
800.0
1000
1200
1400
1600
μAU

Figure 3

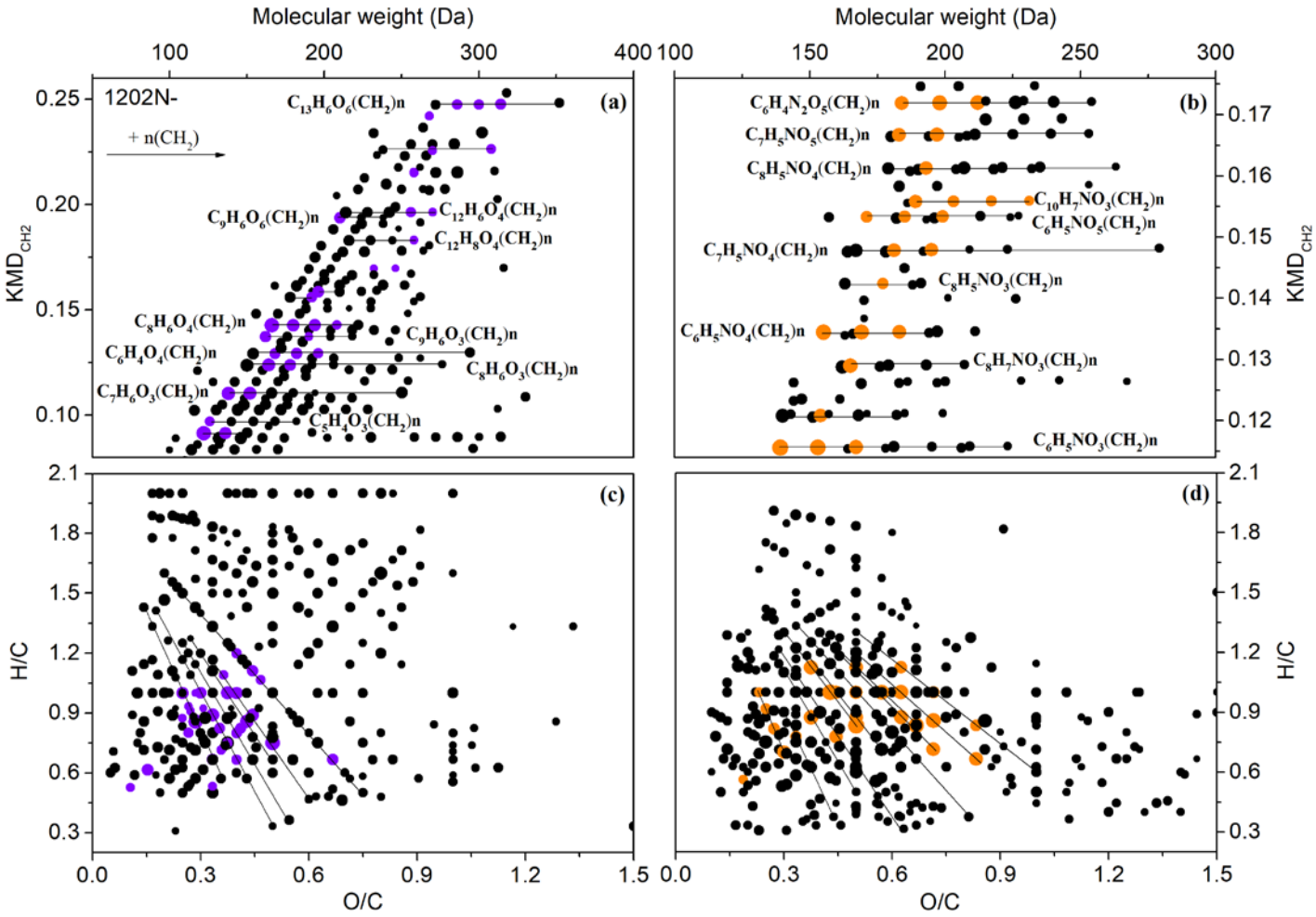
Molecular weight (Da)
Molecular weight (Da)
1202N-
+ n(CH2)
(a)
(b)
(c)
(d)
KMDCH2
H/C
O/C
C13H6O6(CH2)n
C9H6O6(CH2)n
C12H6O4(CH2)n
C12H8O4(CH2)n
C8H6O4(CH2)n
C9H6O3(CH2)n
C6H4O4(CH2)n
C8H6O3(CH2)n
C7H6O3(CH2)n
C5H4O3(CH2)n
C6H4N2O5(CH2)n
C7H5NO5(CH2)n
C8H5NO4(CH2)n
C10H7NO3(CH2)n
C6H5NO5(CH2)n
C7H5NO4(CH2)n
C8H5NO3(CH2)n
C6H5NO4(CH2)n
C8H7NO3(CH2)n
C6H5NO3(CH2)n

Figure 4

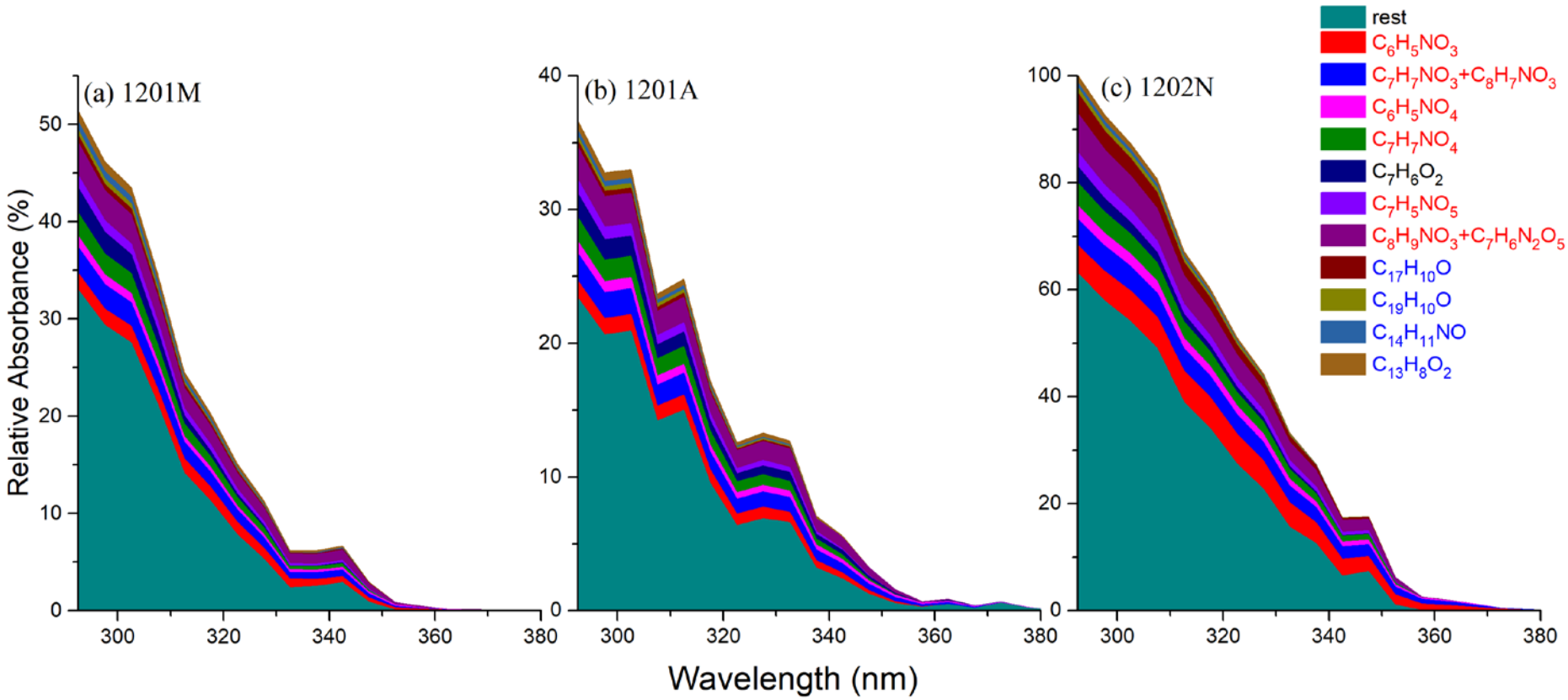

751
752

Figure 5